Journal of Materials Chemistry C

PAPER

View Article Online
View Journal | View Issue

Cite this: J. Mater. Chem. C, 2018, 6, 2556

Tailoring the self-assembling abilities of functional hybrid nanomaterials: from rod-like to disk-like clustomesogens based on a luminescent $\{Mo_6Br_8\}^{4+}$ inorganic cluster core†

Aurore Gandubert,[a] Maria Amela-Cortes,[a] Susanta Kumar Nayak,[a] Cristian Vicent,[b] Cristelle Mériadec,[c] Franck Artzner,[c] Stéphane Cordier[a] and Yann Molard*[a]

Received 26th November 2017,
Accepted 2nd February 2018

DOI: 10.1039/c7tc05412b

rsc.li/materials-c

Self-organizing processes are elegant ways to generate and control the nanostructuration of hybrid materials. We describe in this work the synthesis, self-organizing abilities and photo-physical properties of $(n\mathrm{Bu_4N})_2[Mo_6Br^i_8(L)^a_6]$ clustomesogens containing 18 cyanobiphenyl (CB) mesogenic moieties spread equally around the metallic scaffold *via* aliphatic spacers. By controlling the spacer length and thus the mesogenic density around the rigid inorganic bulky scaffold, we tailored the morphology of hybrid supermolecular building blocks from rod-like to disk-like which strongly influenced their self-organizing abilities. The photophysical properties of hybrids were investigated in their glassy state and in solution. Temperature studies reveal different behaviours depending on the hybrid nanostructuration. Despite their isotropic nature, octahedral clusters offer numerous possibilities in the design of self-assembled hybrid materials showing strong luminescence properties, which is of particular interest in the fields of optics or optoelectronics.

Introduction

Controlling the organization of nanoscale entities within a material is one of the challenges that nanoarchitectonics is willing to tackle.[1] It offers promising perspectives in the design of new materials with tailored properties for various applications in daily life. In that way, the field of hybrid materials has become an intense field of investigations mixing chemistry and physics and gives rise to many materials with applications in optics, microelectronics, batteries, biology, photovoltaics, and medicine.[2] Several strategies enable now the assembly of structurally well-defined nanocomponents into hierarchically organized hybrid architectures. In particular, liquid crystal (LC) nanoscience is an emerging field in the world of hybrid materials, whose main aim is to control the self-assembling ability of some hybrid systems to tailor the molecular arrangement at the molecular scale.[3] Clustomesogens[4] are a class of such hybrid materials. They are defined as transition metal clusters containing hybrid organic inorganic materials that show liquid crystalline behavior. As a sub-class of metallomesogens,[5] they combine the specific properties of metallic clusters (magnetism, redox, luminescence) related to the number of metallic electrons available for metal–metal bonds (VEC)[6] with the anisotropy-related properties of liquid crystals. Nano-sized octahedral metallic clusters found in $[M_6Q^i_8X^a_6]^{n-}$ anionic units (M = Mo, W, or Re; Q = chalcogen/halogen; X = halogen; i = inner, a = apical, $2 \leq n \leq 4$) appear now as an alternative to rare and/or expensive inorganic emitters such as Eu(III), Ir(III) or Pt(II) complexes or quantum dots containing heavy elements. Indeed, recent work reported a luminescence quantum yield of up to 1[7] for such cluster-based materials with a large emission band in the red NIR region able to sensitize the IR luminescence of Er^{3+}, which is of particular interest in telecom applications.[8] Moreover, despite their ionic character, we recently demonstrated the stability of their emission under voltage application.[9] $A_n[M_6Q^i_8X^a_6]$ series (A = alkali cation) are obtained as powders or single crystals by high temperature solid state synthesis in silica containers.[10] Let us stress that octahedral anionic metal clusters can be considered as spherical nano-objects of around 1.2 nm in diameter. Their introduction in a LC matrix is therefore very challenging because their isotropy does not favor molecular disk-like or rod-like geometries that are mandatory to observe mesomorphism. The strategies developed so far consist of

[a] Univ Rennes, CNRS, ISCR – UMR 6226, ScanMAT – UMS 2001, F-35000 Rennes, France. E-mail: yann.molard@univ-rennes1.fr
[b] Servei Central d'instrumentacio Cientifica, Universitat Jaume I Campus de Riu Sec, 12071, Castelló, Spain
[c] Univ Rennes, CNRS, IPR – UMR 6251, F-35000 Rennes, France

† Electronic supplementary information (ESI) available. See DOI: 10.1039/c7tc05412b

associating the metallic scaffold with promesogenic organic ligands designed to interact either by covalent bonding,[4b,4c,11] or electrostatic interactions[12] with the cluster units.[4b,4c,12a,13] Using these techniques, clustomesogens with rod-like geometry were described leading to smectic or nematic phases but no columnar geometry could be achieved yet. Columnar liquid crystals (CLC) are of great interest for the design of smart materials.[14] They are easy to process as thin films and able to spontaneously self-assemble over large areas into highly ordered domains. They show structural defects, self-healing abilities and high charge carrier mobility. Therefore, in terms of applicative prospects, they show high potential in the field of smart materials dedicated to electronic and optoelectronic devices. Photoluminescence in CLC can be provided either by organic discotic molecules, transition metal complexes (blue luminescence with Ag^+ or red luminescence with Pt^{2+} were reported among others)[15] or trivalent lanthanide ions complexed within a functional crown ether scaffold.[16] Luminescent quantum dots were also integrated by simple mixing in CLCs.[17] In all cases, the aim of these studies was to control the polarization of luminescence through the molecular orientation of homeotropically aligned columnar molecular assemblies. To the best of our knowledge, columnar clustomesogens were only very recently obtained by using host–guest supramolecular interactions between the ternary salt $Cs_2Mo_6Br_{14}$ and a 18C-6 crown ether derivative functionalized by two *o*-terphenyl units.[18] We demonstrate in this work that it is possible to control the molecular morphology of clustomesogen hybrid nano-building blocks from rod-like to disk-like and thus their self-assembling processes, by playing with the mesogenic density around the bulky inorganic core.

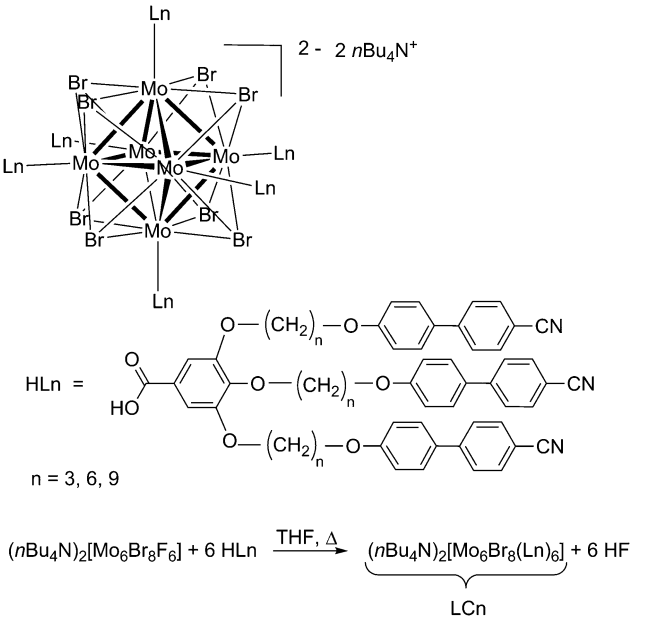

Scheme 1 Representation of the hybrid compounds synthesized in this study.

Results and discussion

Design of hybrid materials

We based the design of our new molecular hybrid material on our previous work which presented the first example of clustomesogens.[4b] These compounds are made of a molybdenum hexanuclear cluster surrounded by eight bromine atoms in the inner position and six apical organic promesogenic ligands. These organic ligands contained terminally appended mesogenic units (cyanobiphenyl, CB) linked to a benzoic acid core by a decyloxy aliphatic chain. Depending on the mesogenic density we were able to show that layered phases and nematic phases could be achieved.[11] As depicted by I. Saez *et al.*,[19] this kind of molecular compound can be defined as a monodispersed polypedal supermolecular material in which the metallic cluster acts as the central hard core scaffold of the dendritic architecture while mesogenic units are terminally attached *via* a spacer chain to this core. In such a case, the self-organization process depends on the density of mesogenic groups, their nature, and on how they are attached (terminally or laterally) to the central core. More particularly for terminally appended mesogenic units such as CB units, a low mesogenic density leads to rod-like supermolecular building blocks that favor layered liquid crystal phases (SmA and SmC),[20] while high mesogenic density should lead to disc-like supermolecular building blocks which should favour columnar arrangement.[19a] Note that similar approaches are already well-known with all-organic materials such as phasmid and polycatenar mesogens and lead to a wide variety of mesophases such as nematic, lamellar or columnar mesophases.[21] Several strategies can be envisioned to increase this density, the one we chose in this work is to shorten the alkyl chain spacer between the CB units and the benzoic acid core. Therefore, we decided to synthesize organic ligands bearing three CB units linked to a benzoic acid unit by alkyloxy chains containing 3, 6 or 9 carbon atoms as depicted in Scheme 1.

Synthesis

$(nBu_4N)_2[Mo_6Br_8F_6]$ was synthesised by following a reported procedure which conforms with the analytical data.[22] The three organic ligands used in this work were synthesized following the same multi-step reaction scheme we used in our previous study. The identity and purity of ligands were assessed by usual techniques such as ^1H and ^{13}C NMR, infrared spectroscopy, mass spectrometry and elemental analysis. Hybrid compounds were obtained by reaction in dry THF of 1 equivalent of $(nBu_4N)_2[Mo_6Br_8F_6]$ and 15 equivalents of the corresponding carboxylic acid derivative. The cluster precursor, originally only poorly soluble in dry THF, became completely soluble after coming in contact with acid. Due to the poor solubility of the carboxylic acid derivatives in acetone, hybrids were purified first by extraction with acetone. Then, pure compounds were obtained by sterical exclusion column chromatography using SX1-Beads swollen in CH_2Cl_2.

The grafting reaction was followed by ^{19}F NMR with the disappearance of the signal located at −10 ppm (in acetone d^6) corresponding to the cluster precursor. The amount of grafted

acid could also be monitored by ^{1}H NMR by comparing the integration values of the signals located at 3.11 ppm corresponding to the methylene protons in the alfa position of the counter cation nitrogen atom and signals located at 4.02 ppm relative to the methylene groups in the α position of the oxygen atoms of the ligand alkyloxy chains. Grafting HL6 and HL3 ligands on the cluster core causes an upfield shift as well as a broadening of their ^{1}H signals, indicating the loss of conformational freedom in solution and pointing out the high steric hindrance around the $\{Mo_6Br_8\}^{4+}$ cluster core. Note that additional well-resolved signals were observed for LC3 in the aromatic region and in the area related to aliphatic protons located in the alpha position of the oxygen atoms around 3.8–4.2 ppm. At first sight, these signals could be interpreted as corresponding to free HL3 although their position is slightly shifted to a higher field. However, the broadness of the signal located at 2.12 ppm corresponding to the aliphatic protons located in the middle of the linker shows that their movement is highly constrained which is not the case for the free ligand. Thus, we can assess that these signals correspond to grafted ligands. IR spectroscopy was used to confirm the absence of free acid by monitoring the carbonyl elongation vibration band located at 1677 cm^{-1} (1714 cm^{-1} for dimers) to 1623 cm^{-1}. ESI(−) mass spectrometry was also used to assess the presence of the hexasubstituted species. These experiments were performed in CH_2Cl_2/MeOH. ESI mass spectra for samples LC3, LC6 and LC9 were very much alike (see Fig. S4, ESI†). In all cases, abundant peaks assigned to the $[LCn - 2nBu_4N]^{2-}$ (n = 3, 6 and 9) dianions were observed and assigned on the basis of their characteristic high m/z values as well as the perfect match between the observed and simulated isotopic distribution patterns. Compounds were further characterized by EDS and elemental analysis. EDS analysis did not reveal the presence of fluorine atoms giving another proof of the full exchange of apical ligands while elemental analysis was concordant with solvated compounds. Indeed, although hybrids were carefully dried at mild temperature (60 °C) under vacuum for 16 hours, solvent molecules possibly trapped within the supermolecules and interacting with the metallic cluster core could not be removed. This behaviour is not unusual in such a bulky dendritic hybrid system.[20c,23]

Physicochemical studies

The mesomorphic properties of hybrid compounds were studied by polarized optical microscopy (POM), differential scanning calorimetry (DSC) and small angle X-ray scattering (SAXS) and compared to the mesomorphic properties observed for their corresponding carboxylic acid precursor. Results are summarized in Table 1 (see the ESI,† Table S2 for HLn data). Depending on the spacer length, hybrid compounds show, as expected, different enantiotropic liquid crystalline behaviours. This behaviour is also completely different from that of their parent carboxylic acid: while HL3 shows an enantiotropic nematic phase in a temperature range of 77 °C, HL6 shows a monotropic nematic phase at higher temperature and in a smaller temperature range (40 °C). For HL9, cooling the acid

Table 1 Phase behaviour, transition temperatures and melting enthalpies of the obtained compounds taken from the 2nd heating cycle

Compound	Transition	T [°C]	ΔC_p[a]	ΔH[b]	$\Delta H/Nb_{CB}$[b]
LC9	g → SmA	17.8	—	—	—
	SmA → I	131.7	—	33.6	1.9
LC6	g → Lam_{Col}	40.8		—	—
	Lam_{Col} → I	158.4	—	32.2	1.8
LC3	g → N_{Col}	65.3		—	—
	N_{Col} → I	122.5	—	13.3	0.7

[a] In kJ mol^{-1} K^{-1}. [b] In kJ mol^{-1}. g: glassy state; N_{Col}: nematic columnar; SmA: smectic A; Lam_{Col}: lamello-columnar; I: isotropic.

at 10 K min^{-1} from its isotropic state induces the formation of a nematic phase followed by a layered phase of SmA type characterised by a typical fan shaped with focal conic defects in the POM texture (see the ESI,† Fig. S11). The temperature range for which mesomorphism is observed varies significantly with the alkyl chain length. All samples underwent three heating/cooling cycles from −20 up to 200 °C to record DSC thermograms. For all hybrids, DSC thermograms show at high temperature broad LC to isotropic state transitions either upon heating or cooling cycles and, at low temperature, a glass transition corresponding to the freezing of the mesophase (see the ESI,† for thermograms). Except for the first heating cycle, all heating and cooling cycles are superimposable meaning that compounds are thermally stable. Such thermal behavior in the first heating cycle is common in supermolecular systems as it was already reported in numerous studies dealing with dendrimers or other supermolecular systems.[19b,20b,24]

The calculated transition enthalpy values are similar for LC9 and LC6, while it is significantly smaller for LC3. At first sight, these values could be seen as very high for LC transition. However, considering the ratio $\Delta H/Nb_{CB}$ in which Nb_{CB} corresponds to the number of CB units within the compound (like in the case of LC dendrimers) gives a better idea of the thermodynamic phenomenon magnitude and allows comparison of our transition enthalpy values with literature data. In that way, calculated enthalpy values are consistent with previously reported enthalpy values for similar transitions. Their increase from LC3 to LC9 suggests that longer spacers allow better ordering of the supermolecular hybrids in the LC phase which is assigned to better decoupling of the mesogens from the rigid core.[19b]

POM observations (Fig. 1, see the ESI,† for full micrographs: Fig. S12–S14) are consistent with DSC thermograms for the isotropic to LC phase transition temperature determination for LC9 and LC6. The LC texture of LC9 that develops upon cooling from the isotropic state presents focal conic fan shaped texture typical of layered phases.

However, if the interpretation of the LC9 texture can be associated with a lamellar phase with no lateral order *i.e.* a smectic A phase, the textures of LC6 and LC3 are more tedious to interpret. At first sight, LC6 texture presents a columnar texture with broken fans however a closer look reveals the presence of few small focal conic defects. Therefore, a lamello-columnar arrangement might be envisioned in this case.

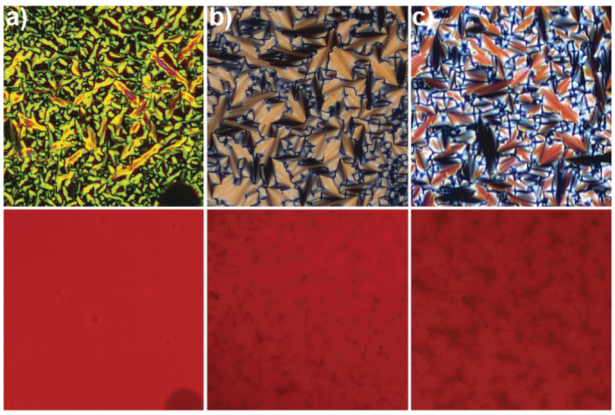

Fig. 1 Polarized Optical micrographs of (a) LC3 (T = 95 °C), (b) LC6 (T = 140 °C) and (c) LC9 (T = 104 °C) hybrids under white light (top) and UV irradiation (bottom).

Due to the high viscosity of LC3, a characteristic texture was rather difficult to develop. Three weeks of annealing between 100 and 95 °C was necessary to observe the fan and homeotropic texture presented in Fig. 1a (other micrographs are presented in the ESI,† Fig. S14) which might be indicative of a columnar arrangement.[25] The majority of the sample remained in a black homeotropic alignment from the isotropic to the LC transition temperature up to 100 °C. To gain a better understanding of the supramolecular arrangement of the three compounds, temperature dependent SAXS experiments were performed. Diffractograms obtained at 100 °C for the three hybrids are presented in Fig. 2 (see the ESI for SAXS patterns at different temperatures). For LC9, the X-ray diffraction patterns recorded at different temperatures within the mesomorphic range are all qualitatively equivalent and contain two sharp small angle reflections characteristic of a layered morphology with a reciprocal spacing in the 1 : 2 ratio. A small shoulder in the 1 : 3 ratio can also be guessed on the diffractogram. Thus, by applying Bragg's law, for instance at 100 °C, a spacing of 41.9 Å attributed to the interlayer lamellar distance was calculated. A diffuse scattering halo in the wide angle region centred around 4.4 Å (h_1) corresponding to the lateral short range order of the molten chains and the cyanobiphenyl moieties confirmed the liquid crystalline nature of the mesophase. X-ray diffraction patterns exhibit additional intense and very broad reflections related to the lateral organization within the inorganic layer. The signal broadness precludes any clear interpretation and shows that clusters are not specifically organized (rectangular or hexagonal lattice) within their layer. Therefore, we can state that LC9 self organizes in a layered phase and that there's no additional order within the inorganic layers. The situation completely differs in the cases of LC6 and LC3 for which only broad signals are detected which implies an order in a much shorter range than the one observed for LC9. For LC3, two signals corresponding to the periodicities of around 32 Å and 14.1 Å (labelled as h in Fig. 2 for the second one) are observed in the diffractograms.

The broadness of the first Bragg signal (and its shift to higher q values with an increase of temperature), the non-appearance of a correlated second order reflection in the LC phase temperature range, and the fact that the position of the reflection labelled h does not depend on temperature, are in good accordance with a nematic columnar organization. Note that in the glassy state at 40 °C, the recorded diffractogram contains a sharper small angle reflection at 33.7 Å with a weak and broad second order reflection at 16.9 Å, and the reflection corresponding to the intercolumnar periodicity (h) which we interpret as a short range order lamello-columnar arrangement in the glassy state. For LC6, the signal corresponding to a periodicity of 14 Å is also observed. Additional shoulders and weak signals in the 1 : 2 reciprocal spacing ratio (black arrow in Fig. 2) are consistent with a short range lamellar periodicity with an interlayer spacing of 38 Å. In order to properly interpret these LC3 and LC6 diffractograms, some geometrical parameters must be considered. Fig. 3 shows the representation according to single crystal X-ray diffraction of a functional cluster unit containing a $\{Mo_6Br_8\}^{4+}$ cluster core bearing six 3,4,5-trimethoxybenzoate derivatives in the apical position.[4b] This unit corresponds to the central rigid core of our

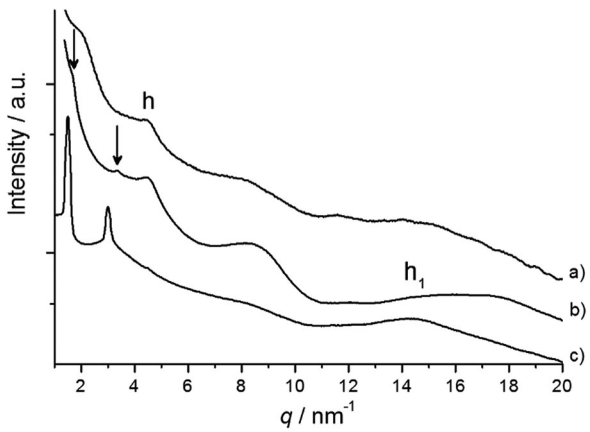

Fig. 2 Small angle X-ray diffraction patterns obtained at 100 °C for (a) LC3, (b) LC6 and (c) LC9.

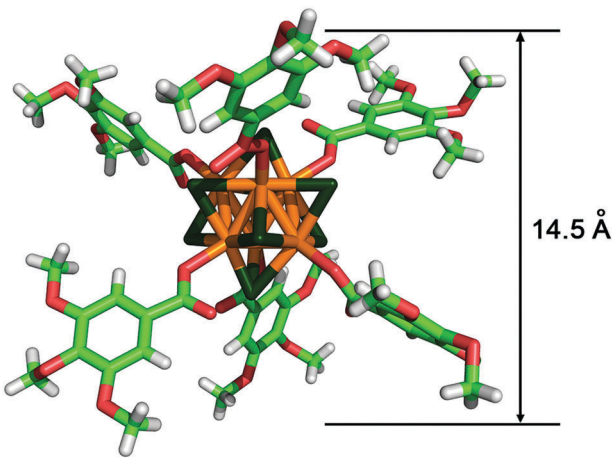

Fig. 3 Representation of the $[Mo_6Br_8(gallate)_6]^{2-}$ derivative according to single crystal X-ray diffraction analysis published in ref. 4b.

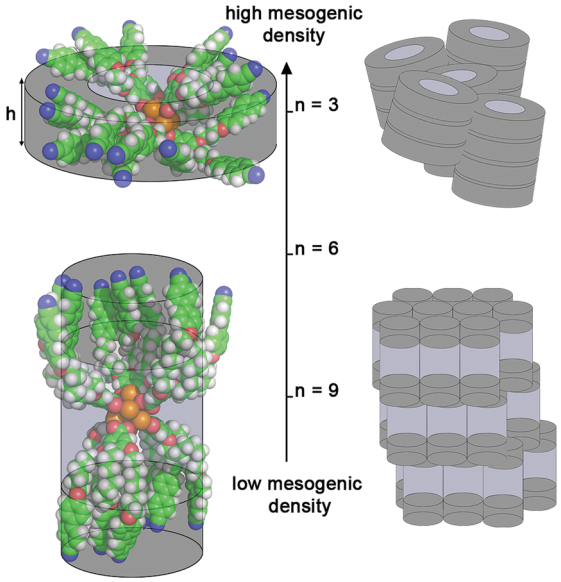

Fig. 4 Schematic representation of LC3 and LC9 nano-building blocks and their self-assembling abilities.

supermolecular systems once methyl groups are removed. In this case, the size of the rigid central core can be approximated to 14.5 Å. With this value being very close to the one deduced from the diffraction patterns of LC6 and LC3 for the (h) signal, we envisioned that (h) corresponds to the intracolumnar periodicity (disc thickness of the hybrids) once they are arranged into a columnar topology (Fig. 4). The diameter of the disc can be deduced for LC3 from the shoulder located around 1.9–1.8 nm^{-1} (note that this signal becomes sharper at 40 °C, ESI†). This corresponds to a diameter of 32–34 Å and is consistent with molecular models obtained using Hyperchem software. In the case of LC6, the diameter of the supermolecular system can be deduced from the diffractograms with the shoulders corresponding to the layer structuration (38 Å at 100 °C). We can note that there is only a little difference between the diameters of LC3 and LC6 deduced from SAXS measurements. This could be explained by the interdigitation of CB moieties in the case of LC6 that could not occur so easily in LC3 because of the high density of CB units around the cluster core that implies a more dense packing of the CB units.

Thus, keeping short the spacer between the metallic scaffold and the mesogenic unit prevents the decoupling of the mesogenic motion from the metallic core and forces the mesogens to pack closely together around the cluster. As a result LC3 self-organizes into a disk shaped geometry. By lengthening the spacer, decoupling occurs allowing the interdigitation of adjacent CB units, up to a full decoupling when a C9 spacer is used. Therefore, the morphology of LC9 (rod like) and LC3 (disk like) is very clear, and an intermediate situation is observed for LC6. These results highlight that the self-assembling process is predominantly driven by the cluster cores for short alkyl spacers while their role is minimized for longer spacers.

Luminescence properties measurements

Molybdenum transition metal clusters are now well known luminophores in inorganic chemistry.[26] Their size (1.2 nm), their composition (no heavy metal like Pb or Cd), the commercial availability of their precursors (molybdenum is a common element in nature) and their luminescence performances (note that very high quantum yields have been recently reported for such compounds)[7,27] indicate that they are a realistic alternative to other inorganic red luminescent dyes such as quantum dots, rare earth trivalent Eu or transition metal ions such as Ir^{3+} or Pt^{2+}. Absolute quantum yield (AQY) measurements were realized at 25 °C, irradiating samples in the glassy state under air or in a N_2 atmosphere (Table 2). Modifying the excitation wavelength has only a little impact on the AQY values (inset Fig. 5). However, AQY values measured in air vary significantly from one hybrid to another. As hybrids are made of the same cluster core bearing gallate derivatives, similar AQY could have been expected for the three hybrids. Measurements, realized in a N_2 saturated atmosphere, followed the same trend indicating that these variations cannot be due to a difference in the material gas permeability implying a different exposure to surrounding oxygen.[28] Considering that hybrids only differ in the spacer chain length between the CB units and the cluster core, we might impart these differences to possible interactions between the blue emissive CB units and the cluster core. This last assumption correlates well with the emission lifetime decays calculated in deaerated solution.

Emission decays were recorded by exciting samples at 375 nm in the glassy state or in diluted deaerated dichloromethane solutions ($c = 10^{-5}$ mol l^{-1}). The data, collected in Table 2, were fitted to a one- or two-exponential decay and the goodness-of-fit judged by the χ^2 values (0.99–1.06) and the residual distribution. All calculated lifetimes are in the range of several microseconds confirming the usual phosphorescence behavior of the cluster core. The LC9 cluster emission decay profile could be fitted with one component (with a lifetime value in the range of those already reported for compounds containing the $\{Mo_6Br_8\}^{4+}$ cluster core)[29] while LC6 and LC3 emission decays contain two components. Thus, in solution, the cluster core might interact with the grafted CB units for C3 and C6 spacers while no interactions are evidenced for a C9 spacer. In the glassy state, however, a biexponential behaviour, independent of the spacer length, is observed. Note that in this case, measurements could only be performed in an air atmosphere. Therefore, interactions with oxygen can be expected and might explain the presence of a second and shorter lifetime component in the emission decays as we already previously observed for other cluster compounds.[12d,27a]

Table 2 Absolute quantum yields calculated at 365 nm in the glassy state at 22 °C and kinetic parameters obtained under 375 nm irradiation in the glassy state and in deaerated CH_2Cl_2 solution

		Kinetic parameters					
	Φ_{em}	Glassy			Deaerated solution		
	Air/N_2	τ_1/μs (%)	τ_2/μs (%)	χ^2	τ_1/μs (%)	τ_2/μs (%)	χ^2
LC3	0.21/0.23	61 (0.47)	161 (0.53)	1.06	31 (0.12)	77 (0.88)	0.99
LC6	0.24/0.33	75 (0.36)	179 (0.64)	0.99	21 (0.92)	51 (0.08)	0.99
LC9	0.09/0.12	50 (0.56)	102 (0.44)	1.03	113	—	0.99

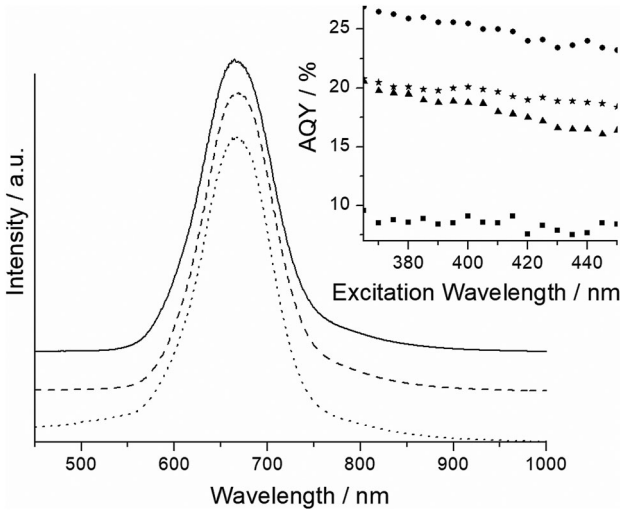

Fig. 5 Emission spectra of LC3 (plain line), LC6 (dashed line) and LC9 (dotted line) observed for λ_{exc} = 380 nm. Inset absolute quantum yields in air of $(n\mathrm{Bu_4N})_2[\mathrm{Mo_6Br_8F_6}]$ (star), LC3 (triangle), LC6 (disk) and LC9 (square) at various wavelengths.

Hybrids were deposited on a microscope slide and their emission abilities vs temperature were studied by using a polarized microscope equipped with a hot stage, an irradiation source and a CCD photodetector. Spectra were recorded upon heating up to 20 °C above their LC to isotropic transition temperature to observe their behaviour around their clearing temperature (see the ESI,† Fig. S20). The three hybrid compounds show a similar large band photoluminescence emission spectrum with a maximum located around 680 nm (Fig. 5). Increasing the temperature induces a decrease of the emission intensity due to higher non-radiative deactivation of the excited state without any shift of the emission maximum. Note that only for LC9, a broad and faint signal centred at a lower wavelength was observed at high temperature and might correspond to the residual emission of CB units. Although the same isotropic cluster core is used in the three hybrids, the decrease of their emission intensity vs temperature does not follow the same trend (see the ESI,† Fig. S21) which could be attributed to their different nanostructurations.

Conclusions

We show in this work how we can tailor the molecular morphology of hybrid molecular nanobuilding blocks to control their self-assembling abilities. In particular, we present the synthesis and studies of the first disc-like clustomesogens designed by a covalent approach. These compounds were obtained by increasing the mesogenic density around the central inorganic luminescent scaffold as compared to previously reported results by shortening the aliphatic spacer between the mesogenic promoter and the rigid bulky metallic scaffold. A long alkyl spacer allows a full decoupling of the mesogenes from the rigid core which does not influence significantly the mesomorphic properties of the hybrid. Shortening the spacer increases the role of the metallic scaffold in the supermolecular system and, as a result, induces the formation of molecular disc-like arrangements whose thickness corresponds to the thickness of the rigid metallic core. These compounds represent one of the very rare examples of supermolecular or dendritic materials containing a rigid central core and terminally appended mesogenic units that show a columnar mesomorphism. This study constitutes a great step in the development of the clustomesogen field as now, all structural requirements have been discovered with CB units to obtain nematic, layered or columnar arrangements. Luminescence studies realized at various temperatures for the hybrids show that they possess the same emission profiles with a large emission between 550 nm and 900 nm and with a maximum around 680 nm. As expected, the metal cluster intrinsic luminescence properties are retained in the hybrid with AQY values and emission lifetimes depending on the cluster core interactions with CB units, which is correlated with their spacer length. This work demonstrates the numerous possibilities offered by transition metal clusters in the design of self-assembled hybrid materials showing strong luminescence properties. It shows that despite their isotropic nature, octahedral clusters can be involved in the formation of anisotropic hybrid molecular compounds once modified covalently with carefully designed organic ligands. These studies open wide perspectives in the design of new anisotropic metal clusters containing hybrid nano-building blocks and thus in the control of self-organization processes within the hybrid materials.

Experimental section

Experimental techniques

NMR spectra were recorded on a Bruker Avance 400P or Brucker Avance 300P. All peaks were referenced to the methyl signals of TMS at δ = 0 ppm. For the ESI-MS study of samples LC3, LC6 and LC9, a QTOF Premier instrument with an orthogonal Z-spray electrospray interface (Waters, Manchester, UK) was used. Nitrogen as a drying and cone gas was used at a flow rate of 300 and 30 L h^{-1}, respectively. A capillary voltage of 3.3 kV was set in the negative scan mode, and the cone voltage was varied from 25 to 150 V. For these Mo_6-based compounds, ion abundances of the identified $[LCn]^{2-}$ dianions were maximized at cone voltages typically around Uc = 150 V and their peak assignments were facilitated by the occurrence of multiple isotopes at natural abundance for Mo. The instrument was calibrated by using a solution of NaI in isopropanol/water from m/z = 100 to 3400. CH_2Cl_2 : CH_3OH (1 : 1) sample solutions at *ca.* 1×10^{-5} M were introduced through a fused silica capillary directly to the ESI source by means of a syringe pump at a flow rate of 10 μl min^{-1}. Isotopic theoretical patterns were calculated using the MassLynx 4.1 program. InfraRed spectra were recorded in the solid state using a Varian 640-IR FT-IR spectrometer. UV-Vis absorption measurements were performed on a Varian Cary 5000 UV-Vis-NIR spectrophotometer. Elemental Analyses were performed in the CRMPO using a Microanalyser Flash EA1112 CHNS/O Thermo Electron. Polarized optical Microscopy and temperature dependent luminescence measurements were realized using a Nikon 80i polarized

microscope equipped with a Linkam LTS420 hot stage, a Nikon Intensilight irradiation source, a Nikon DS-FI2 digital camera and an ocean optics QE65000 photodetector connected by optical fibers. Two optical filters were used to select the excitation wavelength: either with a bandwidth of 330–380 nm or with a bandwidth of 380–420 nm. Absolute quantum yields were determined using a Hamamatsu H9920-03G set up. Lifetime measurements were realized using a homemade set-up constituted by a pulsed laser diode (Horiba deltadiode λ_{exc} = 375 nm), a Horiba TBox sample chamber, an iHR320 imaging spectrometer and a Hamamatsu C10910 Streak camera mounted with a S20-ER streaktube and a slow single sweep unit. This set-up allows recording time dependent emission on a 135 nm wide emission window from 380 nm up to 950 nm. Time scale ranges from 1.2 ns up to 1 ms. DSC measurements were realized at 10 K min^{-1}, unless otherwise stated, using a DSC 200 F3 Maia NETSCH. Small-Angle X-ray Scattering (SAXS) X-ray diffraction patterns were collected using a Mar345 Image-Plate detector (Maresearch) mounted on a rotating anode X-ray generator FR591 (Bruker-AXS) operated at 50 kV and 50 mA with Cu Kα radiation (λ = 1.541 Å). The sample to detector distance was calibrated by using silver behenate. The X-ray patterns were recorded for a range of reciprocal spacing $q = 4\pi \sin\theta/\lambda$ from 0.05 to 3.1 $Å^{-1}$ or 0.03–1.6 $Å^{-1}$, where θ is the diffraction angle. The experiments performed using the present setup provide accurate measurements of distances between 210 Å and 2 Å. The acquisition time was 1–3 h, depending of the sample. The sample was loaded on a thin Lindemanm glass capillar (diameter 1.0 ± 0.1 mm and thickness 15 μm; GLAS, Muller, Berlin, Germany) and placed in an oven for thermotropic studies. The scattering intensities as a function of the radial wave vector were determined by circular integration.

Synthesis

Starting materials were purchased from Acros, Alfa Aesar and Aldrich, and used without further purification unless otherwise stated. Bio-Beads S-X1 were purchased from Bio-Rad Laboratories, Inc. The $(n\mathrm{Bu_4N})_2[Mo_6Br_8F_6]$ precursor was synthesised using a reported procedure[4b] from the precursor $(n\mathrm{Bu_4N})_2[Mo_6Br_8Br_6]$.[22] The synthesis and analytical data of HL*n* are presented in the ESI.†

Synthesis of compound $(n\mathrm{Bu_4N})_2[Mo_6Br_8(Ln)_6]$ (LC*n*)

15 eq. of HL*n* were dissolved in 10 ml of dry THF. This solution was added dropwise to a solution of 10 ml $(n\mathrm{Bu_4N})_2[Mo_6Br_8F_6]$ (0.011 mmol, 1 eq.) in dry THF. The mixture was stirred and concentrated up to dryness by gentle heating. The obtained solid was dissolved in 10 ml of dry THF and further concentrated up to dryness. This protocol was realized three times. Part of the excess of HL*n* was removed by dissolution of the obtained solid in acetone followed by filtration. The hybrids were then purified by size exclusion column chromatography using Bio-Beads S-X1 swollen in dichloromethane (yield: 25%).

LC3. ^{1}H NMR (400 MHz, CD_2Cl_2, δ): 0.99 (t, J = 7.3 Hz, –CH_3–$_{TBA}$, 24H), 1.41 (m, –CH_2–CH_3–$_{TBA}$, 16H), 1.60 (m, –CH_2–$_{TBA}$, 16H), 2.05–2.30 (m, –CH_2–, 36H), 3.11 (m, –CH_2–N_{TBA}, 16H), 4.15 (m, –CH_2–O, 72H), 6.94 (m, –CH_{ar2}, 36H), 7.35–7.65 (m, –CH_{ar3}, 12H + m, –CH_{ar2}, 36H + m, –CH_{ar1}, 72H). ^{13}C NMR (75 MHz, $CDCl_3$, δ): 14.01 (–CH_3–$_{TBA}$, 8C), 20.32 (–CH_2–CH_3–$_{TBA}$, 8C), 24.43 (–CH_2–$_{TBA}$, 8C), 29.82, 30.73, 30.78 (–CH_2–, 18C), 59.50 (–CH_2–N_{TBA}, 8C), 65.18, 65.43, 65.66, 65.96, 66.18, 70.19, 70.35 (–CH_2–O, 36C), 108.98, 109.05 (–CH_{ar3}, 12C), 110.46, 110.54, 110.65 (–CH_{ar1}–CN, 18C), 115.57 (–CH_{ar2}–CO, 36C), 119.51 (–CN, 18C), 127.44, 127.50 (–CH_{ar1}–C–Ar_2, 36C), 128.74, 128.79, 128.84 (–CH_{ar2}–C–Ar_1, 36C), 131.60, 131.77, 131.92 (–C_{ar2}–Ar_1, 18C), 133.02, 133.10, 133.12 (–CH_{ar1}–C–CN, 36C), 145.45, 145.51 (–C_{ar1}–Ar_2, 18C), 152.54, 153.06 (–C_{ar3}–O, 18 C), 160.11, 160.17, 160.27 (–C_{ar2}–O, 12C), 169.39 (–COOMo, 6C). ESI-MS m/z found: $[LC3 - 2n\mathrm{Bu_4N}]^{2-}$ m/z = 3232.7. Elemental analysis: found: C, 59.89; H, 4.88; N, 3.41%. $C_{362}H_{336}N_{20}O_{48}Mo_6Br_8$, $4CH_2Cl_2$ requires: C, 60.31; H, 4.76; N, 3.84%.

LC6. ^{1}H NMR (400 MHz, CD_2Cl_2, δ): 1.02 (t, J = 7.3 Hz, –CH_3–$_{TBA}$, 24H), 1.38–1.88 (m, –CH_2–CH_2–$_{TBA}$, 16H + m, –CH_2–$_{TBA}$, 16H + m, –CH_2–, 72H + m, –CH_2–CH_2–O, 72H), 3.09 (m, –CH_2–N_{TBA}, 16H), 3.72 (m, –CH_2–O, 72H), 6.91 (m, –CH_{ar2}, 36H), 7.36 (m, –CH_{ar3}, 12H), 7.40–7.70 (m, –CH_{ar2}, 36H + m, –CH_{ar1}, 72H). ^{13}C NMR (75 MHz, CD_2Cl_2, δ): 13.42 (–CH_3–$_{TBA}$, 8C), 19.72 (–CH_2–CH_3–$_{TBA}$, 8C), 23.82 (–CH_2–$_{TBA}$, 8C), 25.86, 25.95, 26.05, 29.23, 29.31, 29.42, 30.33 (–CH_2–, 72C), 58.91 (–CH_2–N_{TBA}, 8C), 68.08, 68.11, 68.77, 68.90, 72.99, 73.16 (–CH_2–O, 36C), 108.08 (–CH_{ar3}, 12C), 109.87, 109.95 (–CH_{ar1}–CN, 18C), 114.93, 114.98 (–CH_{ar2}–CO, 36C), 118.97 (–CN, 18C), 126.82, 126.88 (–CH_{ar1}–C–Ar_2, 36C), 128.15, 128.21 (–CH_{ar2}–C–Ar_1, 36C), 130.82, 130.93, 131.04 (–C_{ar2}–Ar_1, 18C), 132.47, 132.51 (–CH_{ar1}–C–CN, 36C), 140.12 (–C_{ar3}–O′, 6C), 144.97, 145.51 (–C_{ar1}–Ar_2, 18C), 152.24, 152.65 (–C_{ar3}–O, 12C), 159.84 (–C_{ar2}–O, 18C), 172.18 (–COOMo, 6C). ESI-MS m/z found: $[LC6 - 2n\mathrm{Bu_4N}]^{2-}$ m/z 3611.3. Elemental analysis: found: C, 61.76; H, 5.59; N, 3.30%. $C_{416}H_{444}N_{20}O_{48}Mo_6Br_8$, $6CH_2Cl_2$ requires: C, 61.69; H, 5.59; N, 3.41%.

LC9. ^{1}H NMR (400 MHz, CD_2Cl_2, δ): 1.03 (t, J = 7.3 Hz, –CH_3–$_{TBA}$, 24H), 1.40–1.53 (m, –CH_2–CH_2–$_{TBA}$, 16H + m, –CH_2–, 180H), 1.58 (m, –CH_2–CH_2–N_{TBA}, 16H), 1.83 (m, –CH_2–CH_2–O, 72H), 3.20 (m, –CH_2–N_{TBA}, 16H), 4.02 (m, –CH_2–O, 72H), 7.01 (m, –CH_{ar2}, 36H), 7.36 (m, –CH_{ar3}, 12H), 7.56 (m, –CH_{ar2}, 36H), 7.69 (m, –CH_{ar1}, 72H). ^{13}C NMR (100 MHz, CD_2Cl_2, δ): 13.56 (–CH_3–$_{TBA}$, 8C), 19.80 (–CH_2–CH_3–$_{TBA}$, 8C), 23.50 (–CH_2–$_{TBA}$, 8C), 25.99, 26.04, 29.22, 29.25, 29.30, 29.32, 29.41, 29.46, 29.50, 29.60, 30.33, 32.26 (–CH_2–, 126C), 58.86 (–CH_2–N_{TBA}, 8C), 68.18, 69.11, 73.39 (CH_2–O, 36C), 108.22 (–CH_{ar3}, 12C), 110.02 (–CH_{ar1}–CN, 18C), 114.99 (–CH_{ar2}–CO, 36C), 118.97 (–CN, 18C), 124.61 (–C_{ar3}–COOMo, 6C), 126.92 (–CH_{ar1}–C–Ar_2, 36C), 128.24 (–CH_{ar2}–C–Ar_1, 36C), 131.09 (–C_{ar2}–Ar_1, 18C), 132.52 (–CH_{ar1}–C–CN, 36C), 142.56 (–C_{ar3}–O′, 6C), 145.08 (–C_{ar1}–Ar_2, 18C), 152.84 (–C_{ar3}–O, 12C), 159.87 (–C_{ar2}–O, 18C), 170.05 (–COOMo, 6C). ESI-MS m/z found: $[LC9 - 2n\mathrm{Bu_4N}]^{2-}$ m/z 3991.1. Elemental analysis: found: C, 63.48; H, 6.21; N, 3.09%. $C_{470}H_{552}N_{20}O_{48}Mo_6Br_8$, $6CH_2Cl_2$ requires: C, 63.71; H, 6.33; N, 3.12%.

Conflicts of interest

There are no conflicts to declare.

Acknowledgements

Authors thank Fondation Langlois for financial support. A. Gandubert thanks MENSR for financial support. S. K. Nayak acknowledges the FP7-PEOPLE-2011-IIF No. 299527 LH-NAN-LC for financial support. M. Amela-Cortes thanks ANR Clusto-mesogen ANR-13-BS07-0003-01 for financial support. The authors are also grateful to the SCIC of the Universitat Jaume I for providing mass spectrometric facilities.

Notes and references

1 (*a*) K. Ariga, M. Li, G. J. Richards and J. P. Hill, *J. Nanosci. Nanotechnol.*, 2011, **11**, 1–13; (*b*) M. Aono and K. Ariga, *Adv. Mater.*, 2015, **28**, 989–992; (*c*) S. Cordier, F. Grasset, Y. Molard, M. Amela-Cortes, R. Boukherroub, S. Ravaine, M. Mortier, N. Ohashi, N. Saito and H. Haneda, *J. Inorg. Organomet. Polym. Mater.*, 2015, **25**, 189–204.

2 (*a*) C. Sanchez, K. J. Shea and S. Kitagawa, *Chem. Soc. Rev.*, 2011, **40**, 471–472; (*b*) C. Sanchez, P. Belleville, M. Popall and L. Nicole, *Chem. Soc. Rev.*, 2011, **40**, 696–753.

3 H. K. Bisoyi and S. Kumar, *Chem. Soc. Rev.*, 2011, **40**, 306–319.

4 (*a*) Y. Molard, *Acc. Chem. Res.*, 2016, **49**, 1514–1523; (*b*) Y. Molard, F. Dorson, V. Circu, T. Roisnel, F. Artzner and S. Cordier, *Angew. Chem., Int. Ed.*, 2010, **49**, 3351–3355; (*c*) A. S. Mocanu, M. Amela-Cortes, Y. Molard, V. Circu and S. Cordier, *Chem. Commun.*, 2011, **47**, 2056–2058.

5 (*a*) D. W. Bruce, D. A. Dunmur, E. Lalinde, P. M. Maitlis and P. Styring, *Nature*, 1986, **323**, 791–792; (*b*) A. M. Giroud-Godquin and P. M. Maitlis, *Angew. Chem., Int. Ed. Engl.*, 1991, **30**, 375–402; (*c*) R. W. Date, E. F. Iglesias, K. E. Rowe, J. M. Elliott and D. W. Bruce, *Dalton Trans.*, 2003, 1914–1931; (*d*) B. Donnio, D. Guillon, R. Deschenaux and D. W. Bruce, in *Comprehensive Coordination Chemistry II: From Biology to Nanotechnology*, ed. J. A. Mc Cleverty, J. J. Meyer, M. Fujita and A. Powell, Elsevier, Oxford, 2003, vol. 7, pp. 357–627; (*e*) D. Pucci and B. Donnio, in *Handbook of Liquid Crystals*, ed. J. W. Goodby, P. J. Collings, T. Kato, C. Tschierske, H. F. Gleeson and P. Raynes, Wiley-VCH Verlag GmbH & Co. KgaA, 2nd edn, 2014, vol. 5, pp. 175–241.

6 (*a*) T. G. Gray, C. M. Rudzinski, D. G. Nocera and R. H. Holm, *Inorg. Chem.*, 1999, **38**, 5932–5933; (*b*) T. G. Gray, C. M. Rudzinski, E. E. Meyer, R. H. Holm and D. G. Nocera, *J. Am. Chem. Soc.*, 2003, **125**, 4755–4770; (*c*) N. Kitamura, Y. Ueda, S. Ishizaka, K. Yamada, M. Aniya and Y. Sasaki, *Inorg. Chem.*, 2005, **44**, 6308–6313.

7 K. Kirakci, P. Kubat, M. Dusek, K. Fejfarova, V. Sicha, J. Mosinger and K. Lang, *Eur. J. Inorg. Chem.*, 2012, 3107–3111.

8 Y. Molard, C. Labbe, J. Cardin and S. Cordier, *Adv. Funct. Mater.*, 2013, **23**, 4821–4825.

9 M. Prevot, M. Amela-Cortes, S. K. Manna, R. Lefort, S. Cordier, H. Folliot, L. Dupont and Y. Molard, *Adv. Funct. Mater.*, 2015, **25**, 4966–4975.

10 K. Kirakci, S. Cordier and C. Perrin, *Z. Anorg. Allg. Chem.*, 2005, **631**, 411–416.

11 M. Amela-Cortes, F. Dorson, M. Prevot, A. Ghoufi, B. Fontaine, F. Goujon, R. Gautier, V. Circu, C. Meriadec, F. Artzner, H. Folliot, S. Cordier and Y. Molard, *Chem. – Eur. J.*, 2014, **20**, 8561–8565.

12 (*a*) Y. Molard, A. Ledneva, M. Amela-Cortes, V. Circu, N. G. Naumov, C. Meriadec, F. Artzner and S. Cordier, *Chem. Mater.*, 2011, **23**, 5122–5130; (*b*) M. Amela-Cortes, S. Cordier, N. G. Naumov, C. Meriadec, F. Artzner and Y. Molard, *J. Mater. Chem. C*, 2014, **2**, 9813–9823; (*c*) M. Prevot, M. Amela-Cortes, S. K. Manna, S. Cordier, T. Roisnel, H. Folliot, L. Dupont and Y. Molard, *J. Mater. Chem. C*, 2015, **3**, 5152–5161; (*d*) M. Prevot, M. Amela-Cortes, S. K. Manna, R. Lefort, S. Cordier, H. Folliot, L. Dupont and Y. Molard, *Adv. Funct. Mater.*, 2015, **25**, 4966–4975.

13 M. Amela-Cortes, F. Dorson, M. Prévôt, A. Ghoufi, B. Fontaine, F. Goujon, R. Gautier, V. Cîrcu, C. Mériadec, F. Artzner, H. Folliot, S. Cordier and Y. Molard, *Chem. – Eur. J.*, 2014, **20**, 8561–8565.

14 (*a*) M. O'Neill and S. M. Kelly, *Springer Ser. Mater. Sci.*, 2013, **169**, 219–245; (*b*) B. R. Kaafarani, *Chem. Mater.*, 2011, **23**, 378–396; (*c*) R. J. Bushby and K. Kawata, *Liq. Cryst.*, 2011, **38**, 1415–1426; (*d*) S. Laschat, A. Baro, N. Steinke, F. Giesselmann, C. Haegele, G. Scalia, R. Judele, E. Kapatsina, S. Sauer, A. Schreivogel and M. Tosoni, *Angew. Chem., Int. Ed.*, 2007, **46**, 4832–4887.

15 (*a*) T. Sato, H. Awano, O. Haba, H. Katagiri, Y.-J. Pu, T. Takahashi and K. Yonetake, *Dalton Trans.*, 2012, **41**, 8379–8389; (*b*) A. Santoro, A. C. Whitwood, J. A. G. Williams, V. N. Kozhevnikov and D. W. Bruce, *Chem. Mater.*, 2009, **21**, 3871–3882; (*c*) V. N. Kozhevnikov, B. Donnio and D. W. Bruce, *Angew. Chem., Int. Ed.*, 2008, **47**, 6286–6289.

16 S. Suarez, O. Mamula, R. Scopelliti, B. Donnio, D. Guillon, E. Terazzi, C. Piguet and J.-C. G. Buenzli, *New J. Chem.*, 2005, **29**, 1323–1334.

17 S. Kumar and L. K. Sagar, *Chem. Commun.*, 2011, **47**, 12182–12184.

18 (*a*) S. K. Nayak, M. Amela-Cortes, C. Roiland, S. Cordier and Y. Molard, *Chem. Commun.*, 2015, **51**, 3774–3777; (*b*) S. K. Nayak, M. Amela-Cortes, M. M. Neidhardt, S. Beardsworth, J. Kirres, M. Mansueto, S. Cordier, S. Laschat and Y. Molard, *Chem. Commun.*, 2016, **52**, 3127–3130.

19 (*a*) I. M. Saez and J. W. Goodby, *Struct. Bonding*, 2008, **128**, 1–62; (*b*) I. M. Saez, in *Handbook of Liquid Crystals*, ed. J. W. Goodby, P. J. Collings, T. Kato, C. Tschierske, H. F. Gleeson and E. P. Raynes, Wiley-VCH Verlag GmbH & Co. KGaA, 2nd edn, 2014, vol. 7, pp. 211–258.

20 (*a*) C. Tschierske, *Angew. Chem., Int. Ed.*, 2013, **52**, 8828–8878; (*b*) E. Terazzi, G. Rogez, J.-L. Gallani and B. Donnio, *J. Am. Chem. Soc.*, 2013, **135**, 2708–2722; (*c*) E. Terazzi, T. B. Jensen, B. Donnio, K. Buchwalder, C. Bourgogne, G. Rogez, B. Heinrich, J. Gallani and C. Piguet, *Dalton Trans.*, 2011, **40**, 12028–12032.

21 H.-T. Nguyen, C. Destrade and J. Malthete, *Adv. Mater.*, 1997, **9**, 375–388.

22 W. Preetz, D. Bublitz, H. G. Vonschnering and J. Sassmannshausen, *Z. Anorg. Allg. Chem.*, 1994, **620**, 234–246.

23 E. Terazzi, C. Bourgogne, R. Welter, J.-L. Gallani, D. Guillon, G. Rogez and B. Donnio, *Angew. Chem., Int. Ed.*, 2008, **47**, 490–495.

24 (*a*) B. Donnio and D. Guillon, *Adv. Polym. Sci.*, 2006, **201**, 45–155; (*b*) J. W. Goodby, I. M. Saez, S. J. Cowling, V. Gortz, M. Draper, A. W. Hall, S. Sia, G. Cosquer, S. E. Lee and E. P. Raynes, *Angew. Chem., Int. Ed.*, 2008, **47**, 2754–2787.

25 (*a*) F. Artzner, M. Veber, M. Clerc and A.-M. Levelut, *Liq. Cryst.*, 1997, **23**, 27–33; (*b*) X. Zhang, H. Guo, F. Yang and J. Yuan, *Tetrahedron Lett.*, 2016, **57**, 905–909.

26 (*a*) S. Cordier, Y. Molard, K. A. Brylev, Y. V. Mironov, F. Grasset, B. Fabre and N. G. Naumov, *J. Cluster Sci.*, 2015, **26**, 53–81; (*b*) A. W. Maverick, J. S. Najdzionek, D. MacKenzie, D. G. Nocera and H. B. Gray, *J. Am. Chem. Soc.*, 1983, **105**, 1878–1882; (*c*) A. W. Maverick and H. B. Gray, *J. Am. Chem. Soc.*, 1981, **103**, 1298–1300.

27 (*a*) M. Amela-Cortes, S. Paofai, S. Cordier, H. Folliot and Y. Molard, *Chem. Commun.*, 2015, **51**, 8177–8180; (*b*) K. Kirakci, K. Fejfarova, M. Kucerakova and K. Lang, *Eur. J. Inorg. Chem.*, 2014, 2331–2336; (*c*) M. N. Sokolov, M. A. Mihailov, E. V. Peresypkina, K. A. Brylev, N. Kitamura and V. P. Fedin, *Dalton Trans.*, 2011, **40**, 6375–6377.

28 J. A. Jackson, C. Turro, M. D. Newsham and D. G. Nocera, *J. Phys. Chem.*, 1990, **94**, 4500–4507.

29 (*a*) K. Kirakci, P. Kubat, J. Langmaier, T. Polivka, M. Fuciman, K. Fejfarova and K. Lang, *Dalton Trans.*, 2013, **42**, 7224–7232; (*b*) S. Akagi, S. Fujii, T. Horiguchi and N. Kitamura, *J. Cluster Sci.*, 2017, **28**, 757–772; (*c*) S. Akagi, S. Fujii and N. Kitamura, *Dalton Trans.*, 2018, **47**, 1131–1139.

